Rock Mech Rock Eng
DOI 10.1007/s00603-014-0665-y

ORIGINAL PAPER

Estimation of Fracture Toughness of Anisotropic Rocks by Semi-Circular Bend (SCB) Tests Under Water Vapor Pressure

M. Kataoka · Y. Obara · M. Kuruppu

Received: 25 March 2014 / Accepted: 9 October 2014

Abstract In order to investigate the influence of water vapor pressure in the surrounding environment on mode I fracture toughness (K_{Ic}) of rocks, semi-circular bend (SCB) tests under various water vapor pressures were conducted. Water vapor is one of the most effective agents which promote stress corrosion of rocks. The range of water vapor pressure used was 10^{-2} to 10^{3} Pa, and two anisotropic rock types, African granodiorite and Korean granite, were used in this work. The measurement of elastic wave velocity and observation of thin sections of these rocks were performed to investigate the microstructures of the rocks. It was found that the distribution of inherent microcracks and grains have a preferred orientation. Two types of specimens in different orientations, namely Type-1 and Type-3, were prepared based on the anisotropy identified by the differences in the elastic wave velocity. K_{Ic} of both rock types was dependent on the water vapor pressure in the surrounding environment and decreased with increasing water vapor pressure. It was found that the degree of the dependence is influenced by the orientation and density of inherent microcracks. The experimental results also showed that K_{Ic} depended on the material anisotropy. A fracture process was discussed on the basis of the geometry of fractures within fractured specimens visualized by the X-ray computed tomography (CT) method. It was concluded that the dominant factor causing the anisotropy of K_{Ic} is the distribution of grains rather than inherent microcracks in these rocks.

Keywords Anisotropic rock · Elastic wave velocity · Mode I fracture toughness · Semi-circular bend (SCB) test · Water vapor pressure · X-ray CT method

1 Introduction

The fracture of brittle materials is a result of crack initiation and propagation, namely the fracture process. Crack initiation takes place when the stress intensity factor K at a microcrack tip reaches a critical value, called the fracture toughness K_c. After initiation, the fracture propagates and connects to other fractures, and, finally, the material reaches failure. The fracture toughness is one of the mechanical properties indicating resistance to crack initiation. It has been applied as: (a) a parameter for the classification of rock materials, (b) an index for rock fragmentation, and (c) a material property in the interpretation of geological features and in the stability analysis of rock structures, as well as in modeling the fracturing of rocks (Whittaker et al. 1992). Estimation of the fracture toughness is important in order to understand the brittle fracture behavior of rocks.

The fracture toughness of rocks is known to be affected by the surrounding environment. Many experiments have been conducted under various surrounding conditions, such as temperature, humidity, and confining pressure (Meredith and Atkinson 1985; Al-Shayea et al. 2000; Al-Shayea 2002; Funatsu et al. 2004; Obara et al. 2006, 2007; Kataoka et al. 2011, 2012). Among these conditions, Obara et al. (2006, 2007) have focused on the effect of water vapor on the fracture toughness of rocks, determined using semi-

M. Kataoka (✉) · Y. Obara
Kumamoto University, 2-39-1 Kurokami, Chuo-ku, Kumamoto 860-8555, Japan
e-mail: 127d9401@st.kumamoto-u.ac.jp

M. Kuruppu
Curtin University, Locked Bag 30, Kalgoorlie, WA 6433, Australia

Published online: 27 October 2014

circular bend (SCB) tests (Chong and Kuruppu 1984; Kuruppu et al. 2014) under various water vapor pressures. It was found that the fracture toughness of andesite and basalt was dependent on the water vapor pressure and decreased with increasing water vapor pressure. This tendency was also shown in the uniaxial compressive strength and tensile strength of rocks. Jeong et al. (2007) and Kataoka et al. (2013) concluded that this phenomenon occurred due to stress corrosion of rocks promoted by the water vapor in the surrounding environment. Stress corrosion is a chemical reaction activated by the stress concentration at a microcrack tip (Freiman 1984; Atkinson and Meredith 1987). Therefore, it can be considered that the stress corrosion of rocks is affected by the microstructure characteristics of rocks, such as density and orientation of inherent microcracks, and types, size, and distribution of mineral grains. Stress corrosion is a significant phenomenon that causes deterioration of many earthen structures, such as slopes and underground openings, in the presence of a moist environment.

It is also considered that the microstructures induce anisotropy on the physical properties of rocks. For example, crystalline rocks such as granite have anisotropic properties causing differences in the elastic wave velocity, uniaxial compressive strength, tensile strength, and fracture toughness in different directions (Lee et al. 2001; Nasseri and Mohanty 2008). The anisotropy can be attributed to the existence of preferred orientations of the microcrack distribution (Schedl et al. 1986). As the microcrack distribution that supports microscopic crack initiation is influenced by the microstructure of rock, the fracture toughness seems to be affected by the microstructures. Accordingly, the influence of the microstructures on the anisotropy of the fracture toughness should be investigated.

Several tests have been proposed to estimate the mode I fracture toughness of rocks, namely the chevron bend (CB) test (Ouchterlony 1980; ISRM Testing Commission 1988), the single-edge-cracked round bar in bending test (Ouchterlony 1981), the short rod (SR) test (Barker 1977; ISRM Testing Commission 1988), the central straight through Brazilian disk test (Atkinson et al. 1982), the cracked chevron-notched Brazilian disk (CCNBD) test (Fowell and Chen 1990; ISRM Testing Commission 1995), the SCB test, and the straight-notched disk bending test (Tutluoglu and Keles 2011). The International Society for Rock Mechanics (ISRM) (1988, 1995) suggested CB, SR, and CCNBD tests for the determination of the static fracture toughness of rocks. The SCB test was added to the suggested methods in 2014 (Kuruppu et al. 2014).

In this research, the fracture toughness of two types of anisotropic rocks, African granodiorite (AG) (Kataoka et al. 2011, 2012) and Korean granite (KG) (Kataoka et al. 2012), was determined under various water vapor pressures, and its dependence on the water vapor pressure of the surrounding environment was investigated. The SCB test was chosen to estimate the fracture toughness of the rocks for its simplicity of specimen preparation, equipment, and testing procedure. Detailed observation of fractures within fractured specimens was performed after the SCB tests. The fracture process was discussed and the influence of the microstructure of the rock on the anisotropy of the fracture toughness was examined.

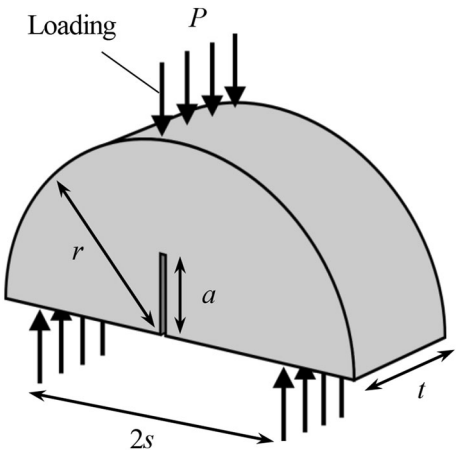

Fig. 1 Semi-circular bend (SCB) specimen and loading configuration

2 Semi-circular Bend (SCB) Test

2.1 Outline

The geometry of the SCB specimen is shown in Fig. 1. This test was developed by Chong and Kuruppu (1984). The SCB specimen is typically core-based and requires relatively little machining effort. In particular, its compact shape formed by cutting a core into slices and duplicated half semi-circular disks is suitable for conveniently investigating the effect of various parameters such as strain rate, moisture content, and temperature on the fracture toughness of rocks (Karfakis 1986). The mode I fracture toughness K_{Ic} is estimated using the following equation (Kuruppu et al. 2014):

$$K_{Ic} = \frac{P_{max}\sqrt{\pi a}}{2rt} Y_I \quad (1)$$

where a, r, and t are an artificial notch length, radius, and thickness of the specimen, respectively. P_{max} is a maximum load. The normalized stress intensity factor Y_I is dimensionless and given as a function of a dimensionless notch length a/r and a half of the support span to radius ratio s/r (Kuruppu et al. 2014).

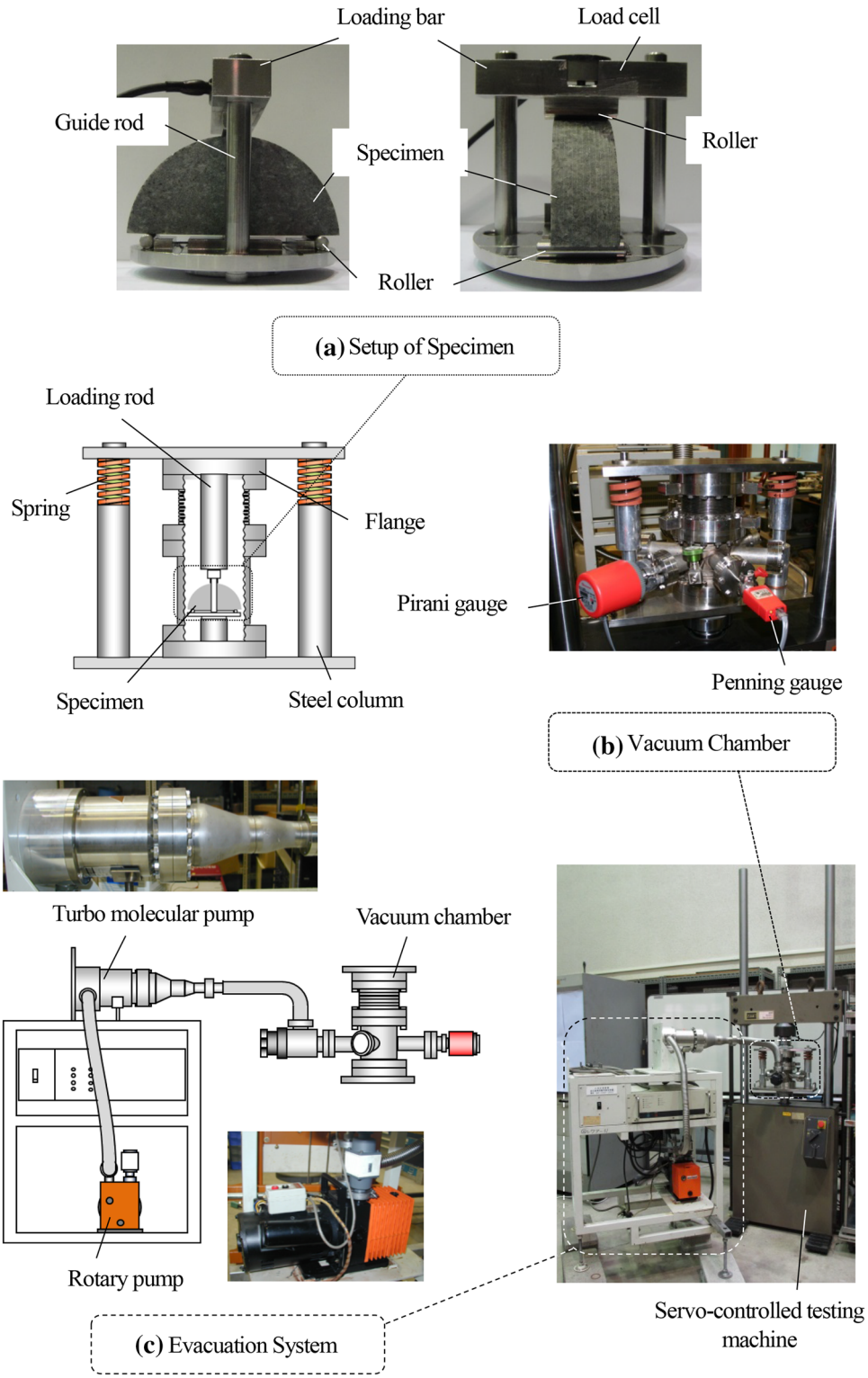

Fig. 2 Testing system. **a** Setup of the specimen with loading apparatus placed inside the vacuum chamber. **b** Vacuum chamber used to control the surrounding environment of the specimen. **c** Evacuation system consisting of a rotary pump and a turbo molecular pump (Kataoka and Obara 2013)

2.2 Experimental Method

The setup of the specimen for the SCB test using a three-point bend type loading apparatus is shown in Fig. 2a. The specimen was placed on the two bottom support rollers with a support span width of 2*s*, as shown in Fig. 1. The value of *s*/*r* was 0.8 in these tests. Load was applied vertically through one upper roller and the two bottom rollers. A loading bar with a load cell can move up and down vertically, aided by the guide rods.

Figure 2b shows the vacuum chamber used to control the surrounding environment of the specimen. The chamber, which is made of SUS304 steel, has upper and lower flanges, ports, and a valve for the injection of gases or vapors. One of the ports was used to lead output from the load cell. Another two ports were used to measure the water vapor pressure in the chamber by two types of pressure gauges and one port with a valve was connected to an evacuation system as described below.

The specimen was placed inside the vacuum chamber as shown in Fig. 2b and the chamber was placed in an MTS servo-controlled testing machine with a capacity of 100 kN, as shown in the bottom right of Fig. 2. The chamber has flanges with a loading rod and the specimen was loaded by pressing down the upper flange using the testing machine. The load application was controlled by a constant displacement rate of 0.01 mm/min. The flanges of the chamber are supported by two steel columns with springs, as shown in Fig. 2b. These springs prevent any load application on the specimen while the surrounding environment was controlled by a process mentioned below. The load was recorded using a load cell with a capacity of 10 kN equipped at the loading bar shown in Fig. 2a. The displacement at the upper loading point was measured using a transducer of the testing machine.

It is necessary that the air in the chamber was exhausted and that various quantities of water vapor were provided. The chamber is linked to the evacuation system through a flexible tube as shown in Fig. 2c. It consists of two vacuum pumps: a rotary pump and a turbo molecular pump. The water vapor pressure in the chamber was measured using two pressure gauges as shown in Fig. 2b, namely a Pirani pressure gauge with a measurement range of 10^{-1} to 10^{5} Pa and a Penning pressure gauge with a measurement range of 10^{-6} to 10^{0} Pa. Figure 3 shows the change of pressure in the chamber before and during the loading. At first, the air in the chamber was exhausted using the two pumps until the pressure was reduced to a level lower than 10^{-2} Pa. Then, distilled water was injected through the injection valve to a pressure of about 10^{3} Pa. As a result, the pressure in the chamber became the saturated water vapor pressure at room temperature and the chamber was filled with only water vapor. It is considered that the air in the chamber was fully changed to the new environment, namely the water vapor environment. Finally, the water vapor in the chamber was exhausted again to a required pressure using the evacuation system. After maintaining the required water vapor pressure for about 6 h, the SCB test was carried out.

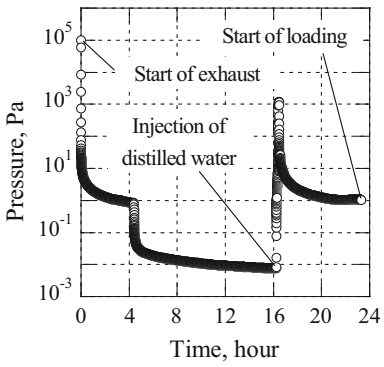

Fig. 3 Change of pressure in the chamber before and during the loading

3 Specimen

African granodiorite (AG) and Korean granite (KG) were used as test materials in this research.

3.1 Preparation of Specimens

The elastic wave velocity v_p was measured in three directions normal to the rock block surfaces shown in Fig. 4. Table 1 shows the results of the wave velocity measurements along three directions defined as Axis-1, Axis-2, and Axis-3 in order of decreasing v_p. Planes perpendicular to each axis were defined as Plane-1, Plane-2, and Plane-3, as shown in Fig. 5. As the v_p results in the direction of Axis-1 are higher than those in the other two directions, this direction of higher v_p can be described to possess lower resistance to the elastic wave propagation. Therefore, many of the inherent microcracks may be presumed to be oriented parallel to Axis-1, as sketched in Fig. 5.

A rock core with a diameter of 75 mm was drilled in the direction of Axis-2 of the blocks, as shown in Fig. 6. Then, the core was sliced into disks with a thickness of approximately 20 mm and each disk was cut into halves to form two semi-circular specimens. Finally, an artificial notch was produced using a diamond blade with a thickness of 0.4 mm. The length of the notch is given by $a/r = 0.5$, where a and r are defined in Fig. 1. The corresponding value of Y_I in Eq. (1) is approximately 6.65. In this paper, two types of specimen were prepared, Type-1 and Type-3, as shown in Fig. 6. The number in the type name represents the direction of the artificial notch and the loading during the test.

The water within specimens should be removed in order to investigate the influence of the water vapor pressure on the fracture toughness of the rocks. In order to achieve a completely dry condition of the specimens, they were kept in an electric drying oven at 100 °C for more than 30 days before the tests.

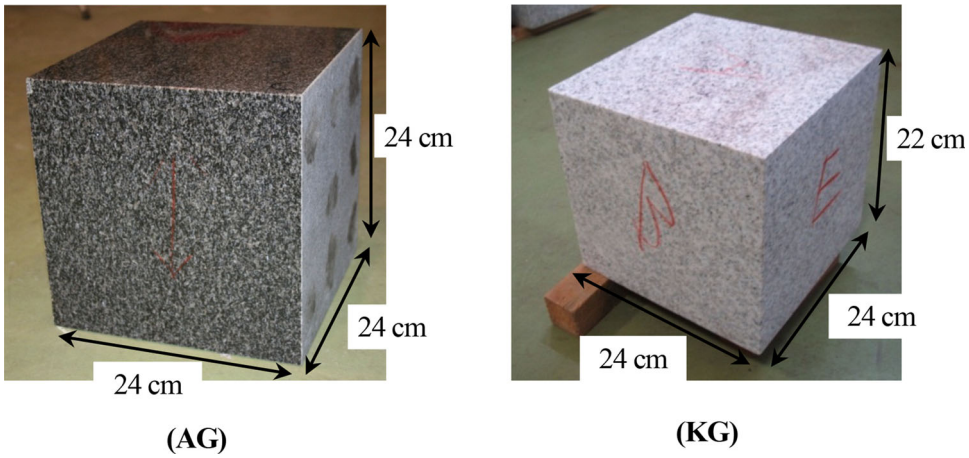

Fig. 4 Blocks of African granodiorite (*AG*) and Korean granite (*KG*)

Table 1 Elastic wave velocity in the directions of the defined axes

	Elastic wave velocity v_p (m/s)		
	Axis-1	Axis-2	Axis-3
African granodiorite	6,760 ± 20	6,580 ± 20	6,540 ± 20
Korean granite	4,180 ± 10	4,120 ± 10	3,960 ± 20

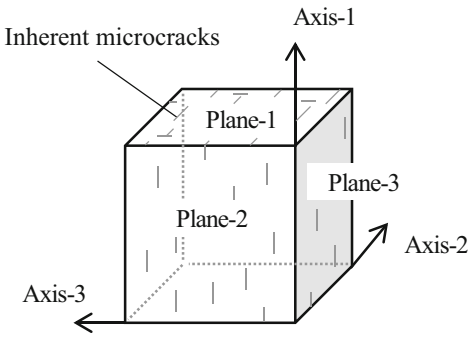

Fig. 5 Definition of axes and planes of the rock block and schematic of the inherent microcracks distribution

3.2 Investigation of Microstructures

In order to investigate the microstructures of rocks, observation of thin sections was performed using a polarization microscope. The thin sections were prepared from three planes: Plane-1, Plane-2, and Plane-3. Figure 7 shows micrographs of the thin sections of both rocks in Plane-2. Mineral grains of plagioclase, amphibole, and biotite in AG and quartz, alkali feldspar, and biotite in KG are observed, respectively. Inherent microcracks can be identified within grains and along grain boundaries. The observed microstructures were analyzed to determine the microcrack density and the average grain diameter in a particular direction.

In order to measure the distribution of microcracks on each plane section, their density was estimated through the following process. Firstly, the angles of all observed microcracks were measured with an accuracy of 1°. The microcracks were then counted on an angle basis at every 20°. Finally, the number of microcracks in a particular direction was divided by the observed area of the plane section (about 1 cm^2) and the microcrack density in that direction was obtained. The results are drawn in rose diagrams as shown in Fig. 8. It is clear that many microcracks are oriented in the direction of Axis-1 and Axis-2 for AG, and the microcrack density in these directions is higher. The tendency of the results is the same as that of the estimation by the elastic wave velocity measurement described in Sect. 3.1. The microcrack density in KG also varies in different principal directions, namely the density of microcracks aligned in the direction of Axis-1 and Axis-2 is higher than that of Axis-3. In addition, the microcrack density in KG is lower than that in AG on the whole and almost the same as the density of microcracks oriented in the direction of Axis-3 in AG (the direction of lower microcrack density).

The intercept method (ASTM International 2010) was used to estimate an average grain diameter d in the three directions. This method consists of drawing a line on the micrographs and counting the number of grains intercepted by the line, as shown in Fig. 9. The length of the line L divided by the number of intercepted grains N ($N = 8$ in Fig. 9), which gives the average grain diameter d. It was applied to each plane and each direction of axes. The results are shown in Table 2. In each plane, an aspect ratio (the ratio of a larger d to a smaller one) was also calculated. The results for AG revealed that d in the direction of Axis-3 is larger than those in other directions in Plane-1 and Plane-2, and that d in the Axis-1 and Axis-2 directions is almost the same as in Plane-3. While KG has smaller differences of d in various directions than AG, d in the

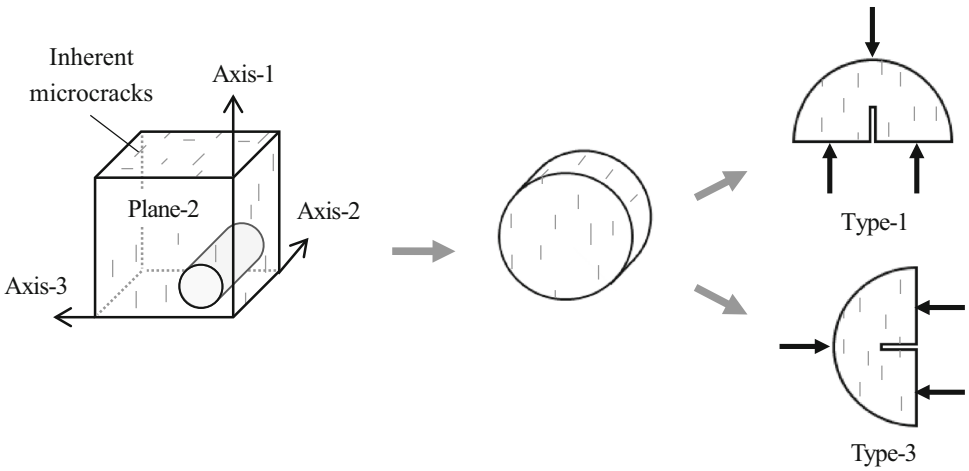

Fig. 6 Schematic of the preparation process for obtaining the two types of specimens

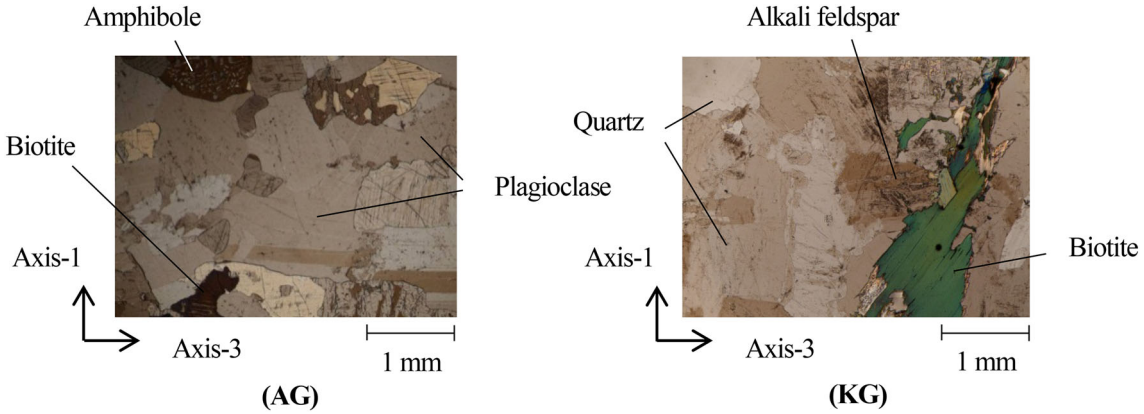

Fig. 7 Micrographs of thin sections (crossed nicols) in Plane-2 for African granodiorite (*AG*) and Korean granite (*KG*) (Kataoka and Obara 2013)

direction of Axis-3 tends to be larger. It shows that the long axes of grains are oriented in the direction of Axis-3. Therefore, the geometry of grain boundaries in the direction of Axis-3 is straighter than that of Axis-1. In addition, the average d of AG is larger than that of KG.

4 Results

The SCB test results and the conditions under which they were performed for both rocks are summarized in Tables 3 and 4. A series of tests was performed using 11 and 14 specimens for Type-1 and Type-3 of AG, and 17 and 15 specimens for Type-1 and Type-3 of KG, respectively. The range of water vapor pressure p in these tests was from 1.0×10^{-2} to 7.7×10^{2} Pa. The fracture toughness K_{Ic} is estimated from the maximum load P_{max} using Eq. (1) described in Sect. 2.

Figure 10 shows examples of the load–displacement curves. In this figure, the curves of both types are shown on the same graph and those of Type-3 are translated 0.1 mm in the positive direction of the horizontal axis for clarity. These curves are downward convex at a low load level and linear until a specimen fractured at P_{max}.

In order to investigate the initiation of the fracture, an SCB test was performed at atmospheric conditions with acoustic emission (AE) monitoring. A specimen of AG Type-3 was used for this test. An AE sensor was attached to a side surface of the specimen. The AE signals were amplified by 40 dB and recorded by a computer with appropriate software (AEwin manufactured by Physical Acoustics Corporation). A threshold of 45 dB was selected and a band-pass filter with a range of 100 kHz to 2 MHz was used. The load and AE event rate during the test are shown in Fig. 11a, b. In Fig. 11b, the load and displacement are normalized by the maximum load P_{max} and a displacement at P_{max}, respectively, and drawn on a magnified scale, shown as the shaded area in Fig. 11a. The AE events are rarely recorded until the load reaches 97.5 % of P_{max} and then the AE rate rises rapidly after the load reaches P_{max}. This result shows that the fracture initiates near P_{max} and propagates rapidly just after the initiation.

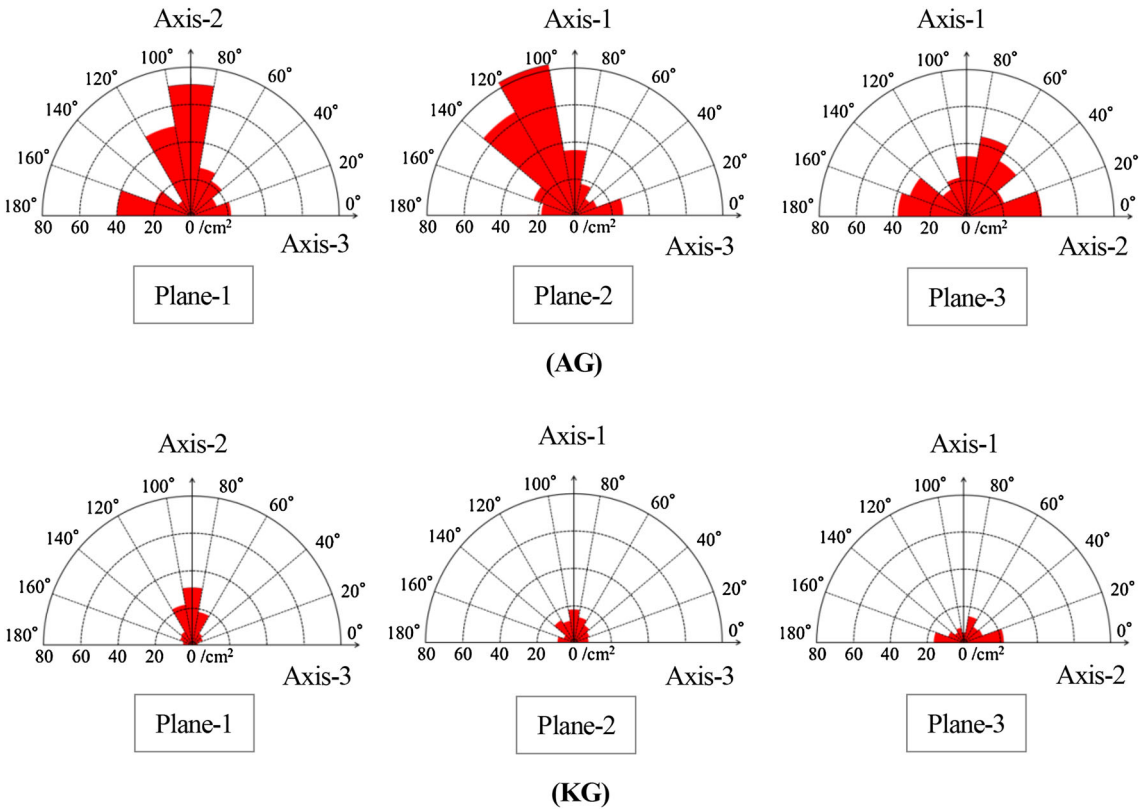

Fig. 8 Microcrack density rose diagrams for African granodiorite (*AG*) and Korean granite (*KG*)

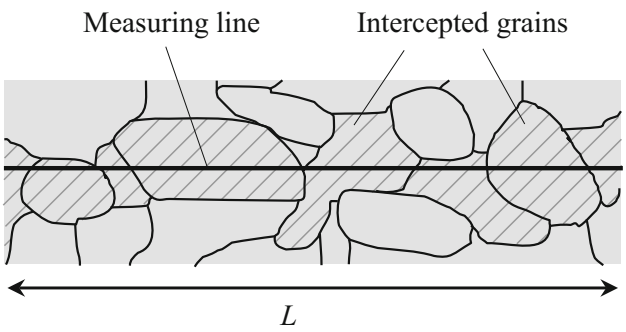

Fig. 9 Schematic of the intercept method

Therefore, P_{max} indicates the loading condition at fracture initiation and can be used for the estimation of K_{Ic} as the critical value of the stress intensity factor K_I in the SCB test.

The relation between the fracture toughness K_{Ic} and the water vapor pressure p is shown in Fig. 12 (refer to Tables 3, 4). K_{Ic} of both the rocks and of the two types investigated in each was plotted against the water vapor pressure p on the logarithmic graph and shown to decrease with increasing p. Lines drawn using least squares approximation are also shown in this figure. The equation of the line is represented as:

Table 2 Average grain diameters of African granodiorite and Korean granite

Plane	Direction	Average grain diameter d (mm)	Aspect ratio
African granodiorite			
Plane-1	Axis-2	0.57 ± 0.11	1.5
	Axis-3	0.84 ± 0.26	
Plane-2	Axis-1	0.62 ± 0.12	1.3
	Axis-3	0.80 ± 0.14	
Plane-3	Axis-1	0.79 ± 0.18	1.1
	Axis-2	0.88 ± 0.29	
Korean granite			
Plane-1	Axis-2	0.66 ± 0.16	1.2
	Axis-3	0.76 ± 0.26	
Plane-2	Axis-1	0.69 ± 0.19	1.0
	Axis-3	0.68 ± 0.13	
Plane-3	Axis-1	0.73 ± 0.17	1.2
	Axis-2	0.63 ± 0.10	

$$K_{Ic} = \beta p^{-m} \tag{2}$$

where β is a constant and indicates K_{Ic} at $p = 1$ Pa on this line. m is a slope of the line on the logarithmic graph and

Table 3 Results of the semi-circular bend (SCB) tests for Type-1 and Type-3 African granodiorite (Kataoka and Obara 2013)

No.	p (Pa)	r (mm)	t (mm)	a (mm)	Y_I	P_{max} (kN)	K_{Ic} (MN/m$^{3/2}$)
Type-1							
1	4.2×10^{-1}	36.7	20.3	17.9	6.63	2.31	2.44
2	7.2×10^{-1}	35.2	21.6	16.3	6.60	2.52	2.48
3	8.5×10^{-1}	36.6	20.2	18.1	6.75	2.22	2.42
4	5.4×10^{0}	37.1	20.2	18.5	6.71	2.23	2.42
5	8.7×10^{0}	36.3	17.8	17.5	6.65	1.96	2.37
6	1.6×10^{1}	36.4	19.9	17.9	6.71	1.80	1.97
7	3.3×10^{1}	36.3	21.5	17.6	6.65	2.32	2.32
8	6.9×10^{1}	36.4	20.3	17.8	6.68	1.98	2.11
9	8.7×10^{1}	35.2	19.0	16.4	6.65	1.97	2.23
10	2.0×10^{2}	35.4	20.1	16.9	6.73	1.89	2.06
11	3.8×10^{2}	36.3	19.0	17.6	6.66	1.73	1.97
Type-3							
1	8.4×10^{-2}	36.2	20.1	17.5	6.68	1.79	1.93
2	2.4×10^{-1}	35.6	17.2	17.2	6.76	1.52	1.95
3	5.2×10^{-1}	36.3	20.1	17.6	6.68	1.62	1.75
4	8.6×10^{-1}	36.7	18.9	18.3	6.75	1.59	1.85
5	1.1×10^{0}	36.4	19.6	17.9	6.71	1.82	2.03
6	2.5×10^{0}	36.1	19.7	17.3	6.63	1.71	1.86
7	4.7×10^{0}	35.7	18.7	16.6	6.55	1.71	1.92
8	1.5×10^{1}	36.1	21.2	17.6	6.73	1.75	1.81
9	3.5×10^{1}	35.8	17.1	17.1	6.65	1.28	1.62
10	4.8×10^{1}	36.4	19.6	17.6	6.65	1.76	1.94
11	9.3×10^{1}	35.8	19.9	17.0	6.63	1.66	1.79
12	1.4×10^{2}	36.1	19.9	17.6	6.73	1.51	1.66
13	4.2×10^{2}	36.8	18.9	17.7	6.53	1.67	1.85
14	7.7×10^{2}	35.7	19.0	16.8	6.61	1.61	1.81

p water vapor pressure, r radius of specimen, t thickness of specimen, a artificial notch length of specimen, Y_I normalized stress intensity factor, P_{max} maximum load, K_{Ic} mode I fracture toughness

indicates the degree of dependence of K_{Ic} on p. These values and correlation coefficients R are summarized in Table 5. The m value of AG Type-1 is higher than the others. Therefore, the influence of p on K_{Ic} for AG Type-1 is the strongest.

Furthermore, the two rocks exhibit anisotropy of K_{Ic} in varying degrees. While many microcracks are oriented in the direction of Axis-1, K_{Ic} of Type-1 is higher than that of Type-3 at the same pressure for both rocks. It is well known that preferentially oriented microcracks result in lower mechanical strength in that direction for rocks. The lower K_{Ic} direction expected based on this knowledge (Axis-1) does not agree with the results that give lower values for Type-3 instead, where the artificial notch is aligned with Axis-3. Moreover, uniaxial compression and Brazilian disk tests were performed using these rocks at atmospheric conditions. These specimens were also prepared for two types, Type-1 and Type-3, where the number in the type name represents the loading direction. Approximately ten specimens were used for the determination of the uniaxial compressive strength and Young's modulus, and five specimens were used for the determination of the tensile strength. Their average values and standard deviations are listed in Table 6. These mechanical parameters also exhibit anisotropic properties and the results are in agreement with that of the SCB tests.

5 Discussion

5.1 Dependence of Fracture Toughness on Water Vapor Pressure

The fracture toughness K_{Ic} is dependent on the water vapor pressure p and decreases with increasing p for both rocks. This tendency is the same for both types of volcanic rock, Kumamoto andesite and Kunnum basalt (Obara et al. 2006, 2007). The decrease of K_{Ic} is due to stress corrosion promoted by water vapor in the surrounding environment. It is concluded that K_{Ic} of rocks is influenced by the stress corrosion.

The m value, the degree of the dependence of K_{Ic} on p, of AG Type-1 is higher than the others, as shown in Table 5. As given in Sect. 3 and shown in Fig. 8 (AG), the

Table 4 Results of the semi-circular bend (SCB) tests for Type-1 and Type-3 Korean granite (Kataoka and Obara 2013)

No.	p (Pa)	r (mm)	t (mm)	a (mm)	Y_I	P_{max} (kN)	K_{Ic} (MN/m$^{3/2}$)
Type-1							
1	1.0×10^{-2}	37.5	19.6	18.6	6.58	1.18	1.28
2	2.1×10^{-2}	37.5	20.2	18.7	6.63	1.26	1.33
3	3.3×10^{-2}	37.5	20.7	18.9	6.69	1.33	1.40
4	4.5×10^{-2}	37.5	20.6	18.7	6.64	1.26	1.31
5	1.8×10^{-1}	37.5	21.4	18.8	6.66	1.36	1.37
6	4.5×10^{-1}	37.5	21.3	18.7	6.61	1.36	1.36
7	1.1×10^{0}	37.5	19.6	18.6	6.60	1.26	1.36
8	3.2×10^{0}	37.5	20.4	18.8	6.66	1.23	1.30
9	4.8×10^{0}	37.5	20.8	19.0	6.72	1.25	1.31
10	1.2×10^{1}	37.5	18.8	18.8	6.65	1.26	1.44
11	1.4×10^{1}	37.5	20.7	18.9	6.70	1.30	1.37
12	2.0×10^{1}	37.5	20.1	18.8	6.66	1.24	1.34
13	8.7×10^{1}	37.5	20.7	18.7	6.63	1.27	1.32
14	1.3×10^{2}	37.5	21.3	18.4	6.54	1.11	1.09
15	2.6×10^{2}	37.5	20.0	19.0	6.71	1.06	1.16
16	4.1×10^{2}	37.5	20.7	18.9	6.69	1.24	1.31
17	5.8×10^{2}	37.5	18.8	18.9	6.69	0.92	1.06
Type-3							
1	1.1×10^{-2}	37.5	21.3	18.3	6.51	1.22	1.20
2	3.2×10^{-2}	37.5	21.3	18.0	6.41	1.18	1.13
3	8.5×10^{-2}	37.5	19.8	18.8	6.66	1.03	1.13
4	1.9×10^{-1}	37.5	21.2	18.8	6.67	1.17	1.19
5	4.6×10^{-1}	37.5	19.9	18.7	6.61	1.13	1.21
6	1.0×10^{0}	37.5	19.8	18.9	6.69	1.09	1.19
7	3.5×10^{0}	37.5	19.1	18.7	6.62	0.91	1.02
8	5.8×10^{0}	37.5	21.3	19.2	6.78	1.07	1.11
9	1.9×10^{1}	37.5	20.2	18.9	6.70	0.98	1.06
10	4.4×10^{1}	37.5	21.4	18.8	6.65	0.98	0.98
11	8.1×10^{1}	37.5	19.3	18.7	6.63	1.05	1.16
12	9.9×10^{1}	37.5	19.4	18.7	6.63	1.00	1.11
13	1.7×10^{2}	37.5	21.3	18.5	6.56	1.15	1.14
14	4.9×10^{2}	37.5	21.6	18.6	6.60	1.00	0.98
15	6.3×10^{2}	37.5	21.3	18.8	6.65	1.10	1.11

p water vapor pressure, r radius of specimen, t thickness of specimen, a artificial notch length of specimen, Y_I normalized stress intensity factor, P_{max} maximum load, K_{Ic} mode I fracture toughness

microcrack density in the direction of Axis-1 is higher than that of Axis-3 for AG. Microcracks aligned in a preferential direction give rise to planes of weakness in rocks. The effect of stress corrosion cracking on such planes can be more severe and the resistance to fracture initiation decreases gradually with increasing water vapor pressure p. Therefore, the m value of Type-1 is higher than that of Type-3 for AG. On the other hand, the m values of Type-1 and Type-3 are almost the same for KG. This rock has lower microcrack density than AG, as shown in Fig. 8, and smaller differences in the respective directions. In addition, the microcrack density of KG is almost the same as that of AG in the direction of Axis-3. Therefore, the m values of KG Type-1 and Type-3, and AG Type-3 are similar to each other. It is found that the m value is dependent on the orientation and the density of microcracks, and that the degree of stress corrosion is sensitive to the microcrack distribution.

5.2 Anisotropy of Fracture Toughness

The rocks used in these tests exhibit anisotropy of the fracture toughness K_{Ic}. The K_{Ic} of Type-1 is higher than that of Type-3 at the same water vapor pressure p. The fracture initiates at the maximum load P_{max} and propagates after reaching P_{max}, as described in Sect. 4. It means that

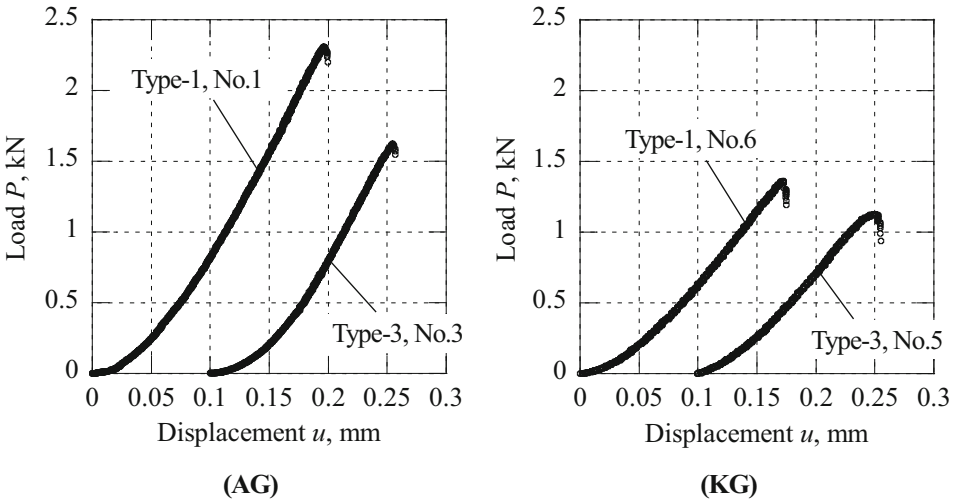

Fig. 10 Load–displacement curves of African granodiorite (*AG*) and Korean granite (*KG*). The curves of Type-3 are translated 0.1 mm in the positive direction of the horizontal axis for clarity

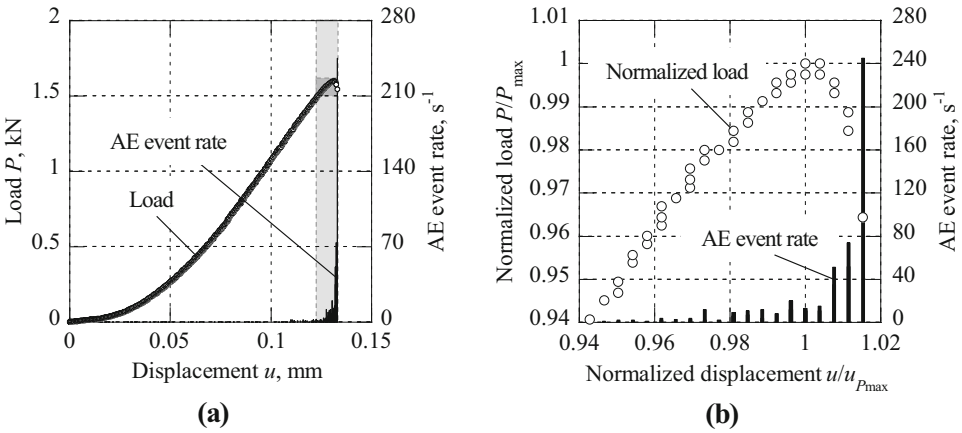

Fig. 11 Semi-circular bend (SCB) test results of African granodiorite with acoustic emission (AE) monitoring: **a** load and AE event rate vs. displacement, and **b** AE event rate and normalized load vs. normalized displacement. The load and the displacement shown in the dark and light gray areas in **a** are given in **b** using normalized scales, along with the AE event rate

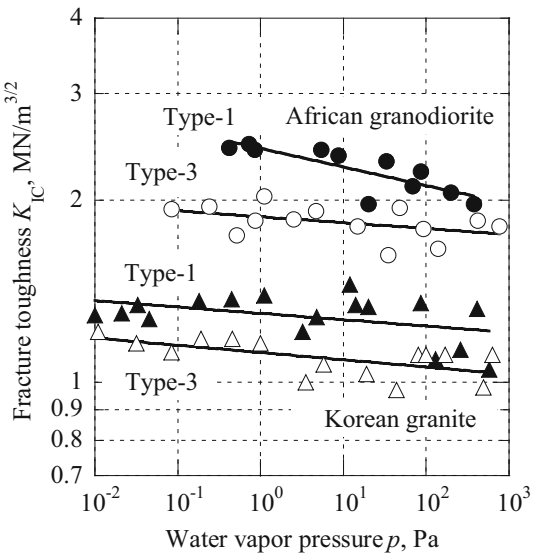

Fig. 12 Relation between fracture toughness and water vapor pressure

Table 5 Parameters of the line [refer to Eq. (2)] shown in Fig. 12 (Kataoka and Obara 2013)

	Type	β	m	R
African granodiorite	1	2.43	0.0301	0.82
	3	1.88	0.0102	0.48
Korean granite	1	1.32	0.0119	0.50
	3	1.13	0.0098	0.52

β constant, m slope of the line on the logarithmic graph, R correlation coefficient

Table 6 Results of the uniaxial compression and Brazilian disk tests

	Type	S_c (MPa)	E_{50} (GPa)	S_t (MPa)
African granodiorite	1	208 ± 29	21.6 ± 0.9	13.9 ± 0.3
	3	205 ± 30	21.4 ± 1.0	11.6 ± 1.5
Korean granite	1	170 ± 22	19.2 ± 0.9	11.4 ± 1.3
	3	167 ± 21	19.0 ± 0.5	10.3 ± 0.7

S_c uniaxial compressive strength, E_{50} Young's modulus, S_t tensile strength

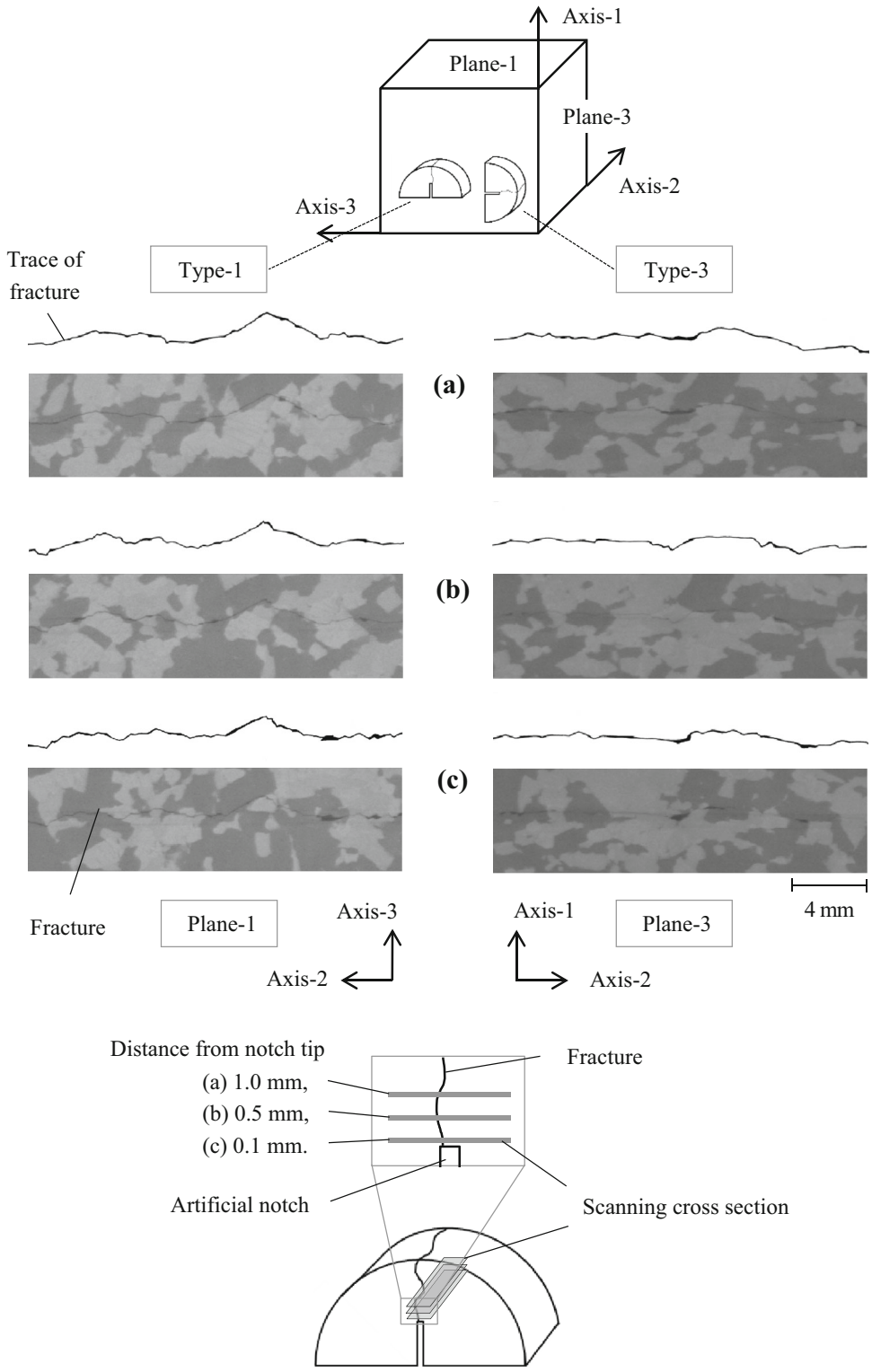

Fig. 13 Computed tomography (CT) scanned images of fractured specimens of African granodiorite obtained at **a** 1.0 mm, **b** 0.5 mm, and **c** 0.1 mm distance from the artificial notch tip. Note that the width of each image is equal to the thickness of the specimen

K_{Ic} corresponds to the point of fracture initiation occurring at the artificial notch tip. Therefore, the fracture geometry observed near the artificial notch tip needs to be considered and related to the fracture initiation of rock.

Following the SCB test, fractured specimens of AG Type-1 and Type-3 were scanned to visualize fractures within the specimens by microfocus X-ray computed tomography (CT) (Mukunoki 2013). The gray-level CT

images of both types of specimens are shown in Fig. 13. The CT images were obtained as cross-sections located at (a) 1.0 mm, (b) 0.5 mm, and (c) 0.1 mm distance from the artificial notch tip and parallel to the notch front, as shown at the bottom of Fig. 13. The images of Type-1 and Type-3 correspond to those taken in Plane-1 and Plane-3, respectively. In the CT images, the dark region shows the area of low density, while the region of relatively light color shows that of high density. The black lines in these images show the gaps, namely the fractures. Traces of the fractures are also shown in this figure. Grain distributions are also observed in the CT images, identified by the difference in density of each mineral. It is found that some parts of the fractures within Type-1 avoid going across grains with higher density (light gray color) and, therefore, the fractures deviate from their intended paths. On the other hand, the geometry of the fractures within Type-3 is straighter than that within Type-1.

As described in Sect. 3, the average grain diameter d in the direction of Axis-3 is larger. It means that the geometry of grain boundaries in the direction of Axis-3 is straighter than in the others for AG. In the CT images of Type-1, as shown on the left side of Fig. 13 (Plane-1), the crack front in the direction of Axis-2, which is perpendicular to the straighter grain boundaries (Axis-3), is given. These fractures have greater deviations in their paths than those within Type-3 shown on the right side of this figure (Plane-3). From this observation of the fracture geometry, it can be found that the fracture tends to initiate along grain boundaries and avoid going through higher density grains (light gray color). That is because the resistance to fracture initiation across higher density grains is higher than if the fractures were to propagate along grain boundaries. Therefore, the fracture toughness K_{Ic} has anisotropic properties and K_{Ic} of Type-1 is higher than that of Type-3 for AG. It is concluded that K_{Ic} is remarkably dependent on the distribution and orientation of grains rather than that of microcracks in this rock. Moreover, it was found that the anisotropic properties of some other crystalline rocks were characterized by the parallel arrangement of grains, especially biotite, amphibole, and/or plagioclase (Kudo et al. 1986, 1992).

The fracture geometry observed on the side surfaces of all fractured specimens was also considered. Figures 14 and 15 show traces of the fractures. They were obtained by tracing the fractures on the photographs of the specimens. The fracture traces of both side surfaces are superposed in these figures. Dashed lines aligned with the directions of artificial notches are also shown. Fracture angles at 0 to 5 mm distance from the notch tips as shown in Fig. 16 were measured. Table 7 shows the results of the measurement. The average fracture angle and the standard deviation of Type-1 are larger than those of Type-3 for both rocks.

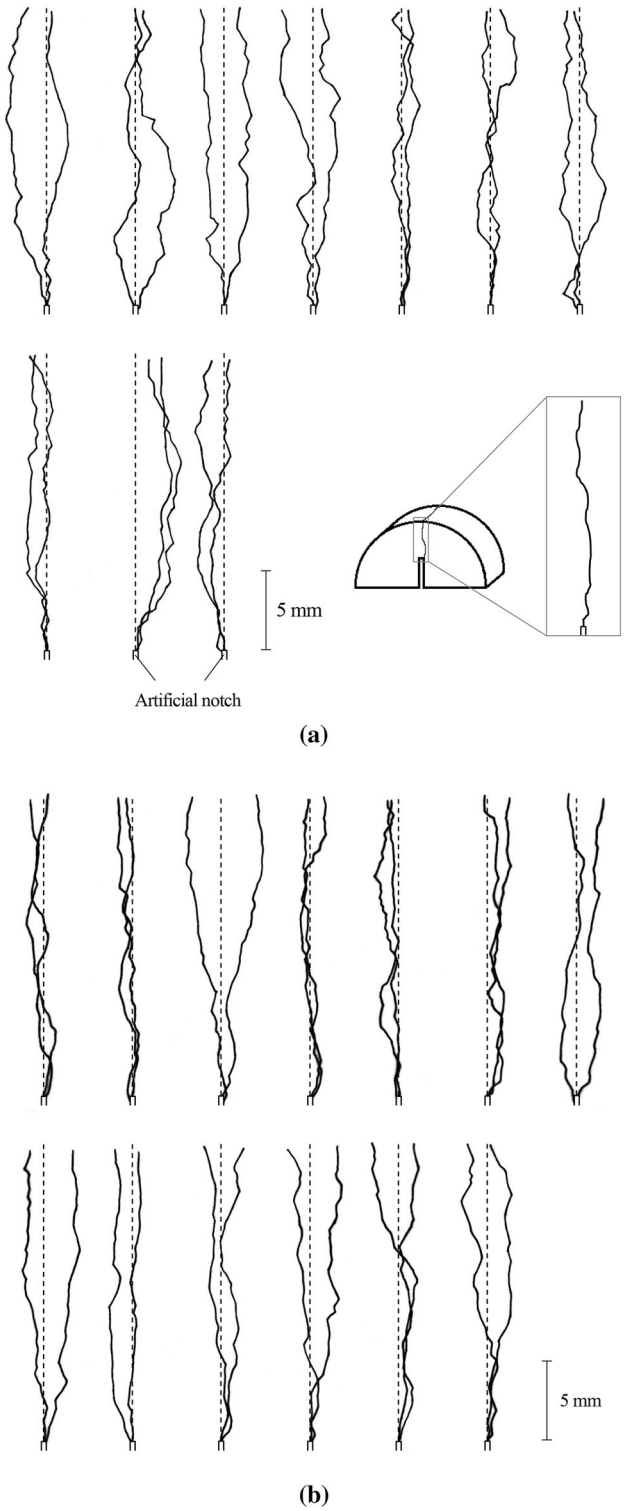

Fig. 14 Traces of fractures observed on the specimen surfaces of African granodiorite: **a** Type-1 and **b** Type-3

The fractures can be expected to propagate in the direction of the artificial notch. According to the results, the smaller fracture angle of Type-3 shows that many of the fractures propagate roughly in the expected direction,

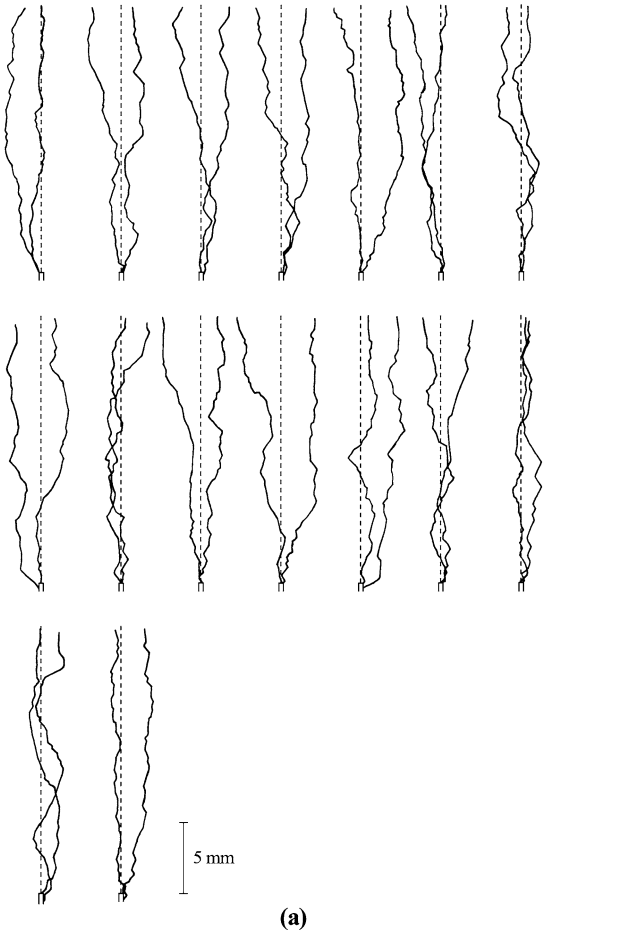

Fig. 15 Traces of fractures observed on the specimen surfaces of Korean granite: **a** Type-1 and **b** Type-3

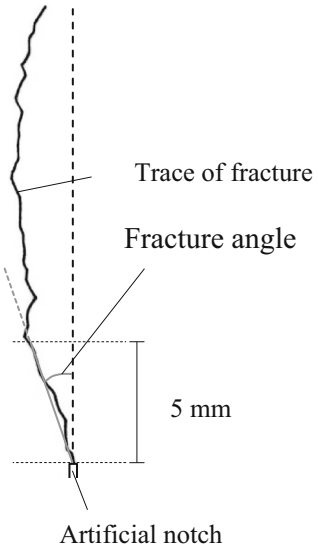

Fig. 16 Definition of fracture angle in Table 7

Table 7 Fracture angle measured in Figs. 14 and 15

	Type	Fracture angle (°)
African granodiorite	1	9.7 ± 6.3
	3	6.4 ± 4.7
Korean granite	1	11.7 ± 5.0
	3	7.7 ± 4.3

namely along the dashed line. On the other hand, the fracture angle of Type-1 is larger, as the fractures propagate away from the dashed line more than that in Type-3. This fracture geometry may be conducive to the existence of greater resistance to fracture propagation in the direction of the artificial notch (Axis-1). As described in Sect. 3, the average grain size in the direction of Axis-3 is larger than that of Axis-1, and the fractures hardly propagate across grains, resulting in the increase of fracture resistance. In the case of Type-3, the fracture propagation is along the lengthwise direction of the grains (Axis-3) and experiences lower resistance than in Type-1. Therefore, K_{Ic} of Type-1 is higher than that of Type-3 because, in that orientation, fractures need more energy to initiate and propagate. This also supports the conclusion that K_{Ic} is dependent on the grain orientation in the rocks used in these tests.

K_{Ic} measured at the microscale will further support any dependence on the effect of material anisotropy. Therefore, it is useful to develop a new laboratory test which can estimate the fracture toughness at the microscale of mineral grains and grain boundaries, namely microscopic K_{Ic} (Kataoka et al. 2014). Furthermore, numerical simulations

of the fracture process are also needed along with the estimated microscopic K_{Ic} in order to investigate the influence of microstructures on the macroscopic K_{Ic} of rocks.

6 Conclusions

The fracture toughness of crystalline rocks and the environment sensitivity to water vapor were investigated in this paper. Firstly, the measurement of elastic wave velocity and the observation of thin sections were performed in the two types of anisotropic rocks, African granodiorite and Korean granite. Then, a series of semi-circular bend (SCB) tests were performed under various water vapor pressures to investigate the influence of the water vapor pressure on the fracture toughness. Furthermore, the fractures within the fractured specimens were observed using the X-ray computed tomography (CT) method following the SCB test. Finally, the influence of microstructures on the anisotropy of the fracture toughness was discussed on the basis of the geometry of the observed fractures. The results are summarized as follows:

1. The preferred orientation of the inherent microcrack and grain distributions can be estimated by measurement of the elastic wave velocity and the observation of the thin sections of the rocks.
2. The fracture toughness K_{Ic} of both the rocks is dependent on the water vapor pressure p and decreases with increasing p. The relation between K_{Ic} and p is represented as

   $$K_{Ic} = \beta p^{-m},$$

   where m indicates the degree of the dependence of K_{Ic} on p.
3. The decrease of K_{Ic} occurred due to stress corrosion promoted by water vapor in the surrounding environment.
4. The m value is dependent on the orientation and density of inherent microcracks.
5. The rock properties elastic wave velocity and fracture toughness displayed anisotropy.
6. On the basis of the fracture geometry visualized by the X-ray CT method, it was suggested that K_{Ic} is dependent on the microstructure of each material. The grain distribution induces anisotropy of K_{Ic} in the rocks tested.

References

Al-Shayea NA (2002) Comparing reservoir and outcrop specimens for mixed mode I–II fracture toughness of a limestone rock formation at various conditions. Rock Mech Rock Eng 35(4):271–291

Al-Shayea NA, Khan K, Abduljauwad SN (2000) Effects of confining pressure and temperature on mixed-mode (I–II) fracture toughness of a limestone rock. Int J Rock Mech Min Sci 37:629–643

ASTM International (2010) ASTM E112-10. Standard test methods for determining average grain size. ASTM, Philadelphia

Atkinson BK, Meredith PG (1987) The theory of subcritical crack growth with applications to minerals and rocks. In: Atkinson BK (ed) Fracture mechanics of rock. Academic Press, San Diego, pp 111–166

Atkinson C, Smelser RE, Sanchez J (1982) Combined mode fracture via the cracked Brazilian disk test. Int J Fract 18(4):279–291

Barker LM (1977) A simplified method for measuring plane strain fracture toughness. Eng Fract Mech 9:361–369

Chong KP, Kuruppu MD (1984) New specimen for fracture toughness determination for rock and other materials. Int J Fract 26:R59–R62

Fowell RJ, Chen JF (1990) The third chevron-notched rock fracture specimen—the cracked chevron-notched Brazilian disc. In: Proceedings of the 31st US Rock Mechanics Symposium, Golden, Colorado, June 1990. Balkema, Rotterdam, pp 295–302

Freiman SW (1984) Effects of chemical environments on slow crack growth in glasses and ceramics. J Geophys Res 89:4072–4076

Funatsu T, Seto M, Shimada H, Matsui K, Kuruppu M (2004) Combined effects of increasing temperature and confining pressure on the fracture toughness of clay bearing rocks. Int J Rock Mech Min Sci 41(6):927–938

ISRM Testing Commission (1988) Suggested methods for determining the fracture toughness of rock. Int J Rock Mech Min Sci Geomech Abstr 25:71–96

ISRM Testing Commission (1995) Suggested method for determining mode I fracture toughness using cracked chevron notched Brazilian disc (CCNBD) specimens. Int J Rock Mech Min Sci Geomech Abstr 32:57–64

Jeong HS, Kang SS, Obara Y (2007) Influence of surrounding environments and strain rates on strength of rocks under uniaxial compression. Int J Rock Mech Min Sci 44:321–331

Karfakis MG (1986) A critical review of fracture mechanics as applied to hydraulic fracturing stress measurements. In: Proceedings of the 1986 SEM Spring Conference on Experimental Mechanics, New Orleans, June 1986, pp 141–147

Kataoka M, Obara Y (2013) Estimation of fracture toughness of different kinds of rocks under water vapor pressure by SCB test. J MMIJ 129:425–432 (in Japanese)

Kataoka M, Obara Y, Kuruppu M (2011) Estimation of fracture toughness of anisotropic rocks by SCB test and visualization of fracture by means of X-ray CT. In: Proceedings of the 12th ISRM International Congress, Beijing, China, October 2011, pp 667–670

Kataoka M, Hashimoto A, Sato A, Obara Y (2012) Fracture toughness of anisotropic rocks by semi-circular bend (SCB) test under water vapor pressure. In: Proceedings of the 7th ARMS, Seoul, Korea, October 2012, pp 458–465

Kataoka M, Obara Y, Jeong HS (2013) Influence of water vapor pressure in surrounding environment on strength and fracture toughness of rocks. In: Proceedings of the ISRM International Symposium EUROCK 2013, Wrocław, Poland, September 2013, pp 21–26

Kataoka M, Ito T, Takashima K, Obara Y (2014) A new testing method to estimate microscopic fracture toughness of rock. In: Proceedings of the ROCKMEC XIth Regional Rock Mechanical Symposium, Afyonkarahisar, Turkey, May 2014, pp 91–96

Kudo Y, Hashimoto K, Sano O, Nakagawa K (1986) The empirical knowledge of quarryman and physical properties of granite. JSSMFE 34:47–51 (in Japanese)

Kudo Y, Sano O, Murashige N, Mizuta Y, Nakagawa K (1992) Stress-induced crack path in Aji granite under tensile stress. Pure Appl Geophys 138:641–656

Kuruppu MD, Obara Y, Ayatollahi MR, Chong KP, Funatsu T (2014) ISRM-suggested method for determining the mode I static fracture toughness using semi-circular bend specimen. Rock Mech Rock Eng 47:267–274

Lee SE, Cho SH, Seo YS, Yang HS, Park HM (2001) The effect of microcracks on the mechanical anisotropy of granite. Mater Sci Res Int 7:7–13

Meredith PG, Atkinson BK (1985) Fracture toughness and subcritical crack growth during high-temperature tensile deformation of Westerly granite and Black gabbro. Phys Earth Planet Int 39:33–51

Mukunoki T (2013) Proceedings of the 4th International Workshop on X-ray CT Visualization for Socio-Cultural Engineering and Environmental Materials X-Earth

Nasseri MHB, Mohanty B (2008) Fracture toughness anisotropy in granitic rocks. Int J Rock Mech Min Sci 45:167–193

Obara Y, Sasaki K, Matsuyama T, Yoshinaga T (2006) Influence of water vapor pressure of surrounding environment on fracture toughness of rocks. In: Proceedings of the 4th ARMS, Singapore, November 2006, chapter 7

Obara Y, Sasaki K, Yoshinaga T, Suzuki Y (2007) Influence of water vapor pressure of surrounding environment on fracture toughness and crack velocity of rocks. In: Proceedings of the 11th ISRM International Congress, Lisbon, Portugal, July 2007, pp 51–54

Ouchterlony F (1980) A new core specimen for the fracture toughness testing of rock. Swedish Detonic Research Foundation Rep DS, Stockholm

Ouchterlony F (1981) Extension of the compliance and stress intensity formulas for the single edge crack round bar in bending. ASTM STP 745:237–256

Schedl A, Kronenberg AK, Tullis J (1986) Deformation microstructures of Barre granite: an optical, SEM and TEM study. Techtonophysics 122:149–164

Tutluoglu L, Keles C (2011) Mode I fracture toughness determination with straight notched disk bending method. Int J Rock Mech Min Sci 48:1248–1261

Whittaker BN, Shingh RN, Sun G (1992) Rock fracture mechanics: principles, design, and applications. Developments in geotechnical engineering. Elsevier, Amsterdam